

**Quantification of macromolecule crowding at single-molecule level**Ting Liang,<sup>1,\*</sup> Chao Yang,<sup>1,\*</sup> Xiaoya Song,<sup>1</sup> Yuyu Feng,<sup>1</sup> Yanhui Liu,<sup>1,†</sup> and Hu Chen<sup>2,‡</sup><sup>1</sup>College of Physics, Guizhou University, Guiyang 550025, China<sup>2</sup>Research Institute for Biomimetics and Soft Matter, Fujian Provincial Key Lab for Soft Functional Materials Research, Department of Physics, Xiamen University, Xiamen 361005, People's Republic of China

(Received 24 March 2023; accepted 19 June 2023; published 20 July 2023)

Macromolecule crowding has a prominent impact on a series of biochemical processes in the cell. It is also expected to promote macromolecular complexation induced by excluded volume effects, which conflicts with recent advances in the thermodynamic interaction between inert, synthetic polymers, and nucleic acids. Along this line, a method combining high-resolution magnetic tweezers and extended crowder-oxDNA model was applied to resolve these discrepancies by systematically studying the kinetics and thermodynamics of the folding-unfolding transition for an individual DNA hairpin in a crowded environment. More specifically, from the magnetic tweezers-based experiments, the linear dependence of the critical force of the DNA hairpin on the polyethylene glycol (PEG) concentration was demonstrated, which is consistent with the results based on the crowder-oxDNA model in which the Lennard-Jones potential was adopted to express the interaction between the crowders and the DNA hairpin. These consistencies highlight that the excluded volume effects are mainly responsible for the interaction between PEG and the DNA hairpin, which is different from the interaction between dextran and the DNA hairpin. In the meantime, the dependence of the folding rate on the molecule weight of PEG, which was different from fluorescence resonance energy transfer-based results, was identified. The proposed method opens a path to detect the interaction between an inert, synthetic molecule, and the DNA hairpin, which is important to accurately mimic the cytosolic environments using mixtures of different inert molecules.

DOI: [10.1103/PhysRevE.108.014406](https://doi.org/10.1103/PhysRevE.108.014406)**I. INTRODUCTION**

The heterogeneous cytosol is composed of biopolymers with different shapes, sizes, and charges, which occupy 20–30% of the cell volume [1–3], even up to 40% for *Escherichia coli* [4,5]. This highly crowded environment in confined space results in strongly reduced and nonrandom diffusion of macromolecules and affects a series of cellular biochemical processes, such as gene expression, cell division, etc. [6–10]. Until now, the impact of the physicochemical properties of the crowded cytosol on the key biochemical processes in the cell has not been clear. Therefore, the intracellular macromolecular crowding effects have attracted the attention of the scientific community.

Macromolecular crowding is typically studied *in vitro* by adding biologically inert and synthetic polymers into a confined space to mimic the cellular environments [11–13]. The early works in the literature [11,12] mainly concentrated on the phase segregation of binary mixtures in a confined space, such as the mixture of DNA and polyethylene glycol (PEG) within an aqueous microspheroid. However, its impact on the biochemical processes of the gene therapy, such as the cleavage of DNA by HindIII enzyme in solutions of PEG 6000 at relatively high concentration values was inhibited by the enhanced formation of the DNA nanoparticles [13]. In the meantime, various types of simulations were performed on the self-entanglement of polymer in the presence of macromolecular

crowding [14–16], indicating that the macromolecular crowding enhanced the incidence of the physical knots by more than an order of magnitude for all considered chain lengths [15]. In addition, these experimental and simulated results were analyzed according to the conventional modeling of the pure molecular crowding dynamics based on hard sphere excluded volume considerations, which explicitly ignored any chemical interactions between the inert, synthetic polymers, and the probes. Nonetheless, the heterogeneous cytosol was replete with nonspecific chemical interactions, both associative and repulsive, which posed the question of whether high concentrations of biologically inert and synthetic polymers in cell-like environments can faithfully mimic cellular environments.

With the implementation of single-molecule techniques for investigating macromolecule crowding effects [12,17–21], such as single-molecule fluorescence resonance energy transfer (smFRET), a series of advances were obtained in studying the thermodynamic interaction between inert, synthetic polymers, and nucleic acids [17,19,20]. Particularly, the macromolecule crowding effects induced by PEG 8000, Ficoll 70, and *E. coli* lysate approximate to the cytosolic conditions were systematically studied based on a FRET-based DNA hairpin structure. From the acquired results, it was pointed out that both PEG 8000 and Ficoll 70 strongly promoted more compact FRET probe conformations and improved the probe FRET efficiency in PEG 8000 or Ficoll 70, which was notably larger than that in *E. coli* lysate at the same concentration (vol%), and enhanced by the increasing concentration (vol%). However, the probe FRET efficiency in Ficoll 70 was lower than that in PEG 8000. In striking contrast, the changing pattern of the probe FRET efficiency with the concentration

\*These authors contributed equally to this work.

†Corresponding author: yhliu1@gzu.edu.cn

‡Corresponding author: chenhu@xmu.edu.cn

of *E. coli* lysate revealed a notable reduction. Nevertheless, it was then gradually recovered to the initial values in the solutions without *E. coli* lysate. This effect was attributed to the competition between the excluded volume interactions and the associative interactions of the crowding agents and the FRET probes [12]. The structural dynamics of DNA hairpins was also further explored by conducting FRET-based experiments in the presence of PEG 6000, Dextran 6000, or Ficoll 70000. From the extracted results, it was indicated that PEG 6000 promoted the DNA hairpin transition by simultaneously increasing the folding rate and decreasing the unfolding rate, while the folding rate was particularly affected. By means of contrast, Dextran 6000 and Ficoll 70000, at similar wt % concentration values with PEG 6000, only resulted in a relatively small increase in the folding rate and a negligible decrease in the unfolding rate [19,20].

Obviously, the cytosolic environments cannot be mimicked by the addition of a biologically inert and synthetic molecule. On top of that, the interactions between inert molecules and probes vary with the species of the inert molecule. The key to resolve these discrepancies among the recent single-molecule experiments on macromolecule crowding is to identify the interaction between the inert, synthetic polymer, and DNA hairpin in crowded environments. Under this direction, in this paper, single-molecule experiments and simulations based on the extended crowder-oxDNA model were combined to identify the interactions between an inert molecule and DNA hairpin at the single-molecule level. The magnetic tweezers were first employed to detect macromolecule crowding effects caused by PEG on the stability of the DNA hairpin. Then, the dependence of the critical forces on PEG concentration was identified by analyzing the force-decendent open probability and folding-unfolding rates. When the crowdiers representing the inert polymers were added to the simulation systems, the interaction potential between the crowder and DNA hairpins was tuned according to the physical characteristics of the inert molecule. Moreover, the extended ox-DNA model could provide the open probability, folding-unfolding rates, and critical forces of DNA hairpins in different crowded environments. These outcomes were further compared with the results obtained in single-molecule experiments based on magnetic tweezers. Consequently, a deep understanding of the interaction between inert polymer and DNA hairpins was obtained, which is of great importance to effectively mimic the cytosolic environments using mixtures of different inert molecules.

## II. MATERIALS AND METHODS

### A. Single-molecule experiment

DNA hairpin structure with a sequence of 5'-GAG TCC TGG ATC CTG TTTT TTTT CAG GAT CCA GGA CTC-3' was linked between two GC-rich double-stranded DNA (dsDNA) handles with lengths of 228 bps and 361 bps, respectively. And the high GC contents of about 63% make them not easy to break during the folding (unfolding) transition process [22–24]. The polymerase chain reaction was applied to produce the two dsDNA handles with bacteriophage  $\lambda$ -DNA (New England Biolabs) as a template. Thiol-labeled forward primer 5'-thiol-AAG CGG GGA TTT CCG TCG GG-3' and reverse primer 5'-ACC GCC AGC

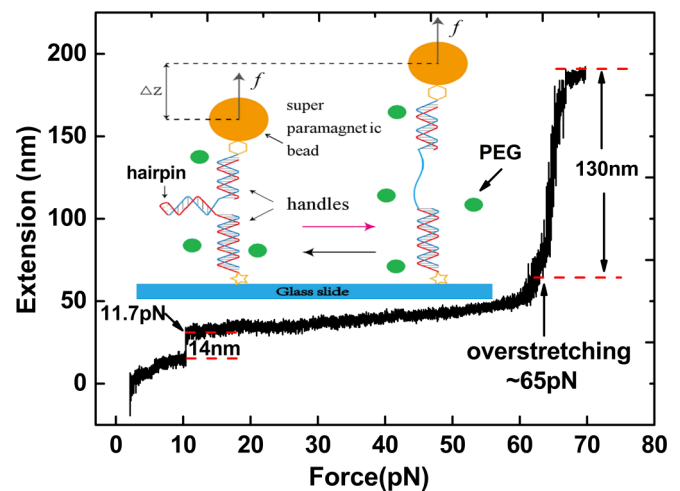


FIG. 1. Force-extension curve of DNA hairpin construct. The inset depicts a sketch of folding-unfolding transitions of a DNA hairpin construction at stretching force. The DNA hairpin sandwiched between two dsDNA handles was linked between a 2.8  $\mu\text{m}$  diameter superparamagnetic dynal bead (M280 bead, Invitrogen) and coverslip surface through specific biotin-streptavidin interaction and sulfo-SMCC crosslinker (Thermo Scientific), respectively. With the increasing force, the extension showed two distinct conformational transitions. The DNA hairpin was unfolded to ssDNA at a force of  $\sim 11.7$  pN, and B-form DNA handles were overstretched to S-form DNA with 70% longer extension at a force of  $\sim 65$  pN.

GAG GTG GCC-3' were used to produce a 228-bp dsDNA handle. Forward primer 5'-ATT ACC ATC TGC CTG GTA TCA GGG C-3' and biotin-labeled reverse primer 5'-bio-GCT CCG CCG ACA CGT GG-3' were used to produce a 361-bp dsDNA handle. BstXI restriction enzyme was added to cut the end of DNA handles to generate sticky ends of four bases ssDNA. Then, the synthesized ssDNA hairpin sequence and two assistant flank ssDNA were mixed with both DNA handles with equal molar concentration [25]. Additionally, T4 polynucleotide kinase (New England Biolabs) was applied to add a phosphate group at the 5' end of synthesized ssDNA. Next, T4 DNA ligase (New England Biolabs) was applied to link the DNA hairpin with two dsDNA handles. Finally, the DNA construct was purified by agarose gel using PureLink gel purification kit (Invitrogen).

As shown by the inset in Fig. 1, the hairpin structure sandwiched between the two handles was linked to a 2.8  $\mu\text{m}$  diameter superparamagnetic dynal bead (M280 bead, Invitrogen) and the coverslip surface through specific biotin-streptavidin interaction and sulfo-SMCC crosslinker (Thermo Scientific), respectively. What's more, the DNA construct was manipulated by magnetic tweezers at different crowding conditions with the concentrations of PEG ranging from 0 to 10%.

The magnetic tweezers were built on an inverted Olympus microscope IX73. An oil-immersion objective (UPLFLN100XO2, Olympus) and a CCD camera (Pike F032B, AVT) were used to image the tethered and reference beads on the coverslip surface. The permanent magnets were moved with two micron resolution by motorized linear stage (LS-110, PI) to control force. The focal plane of the objective was adjusted with nanometer resolution by a piezo objective actuator (PD72Z1CA0, PI) to build the image library, which

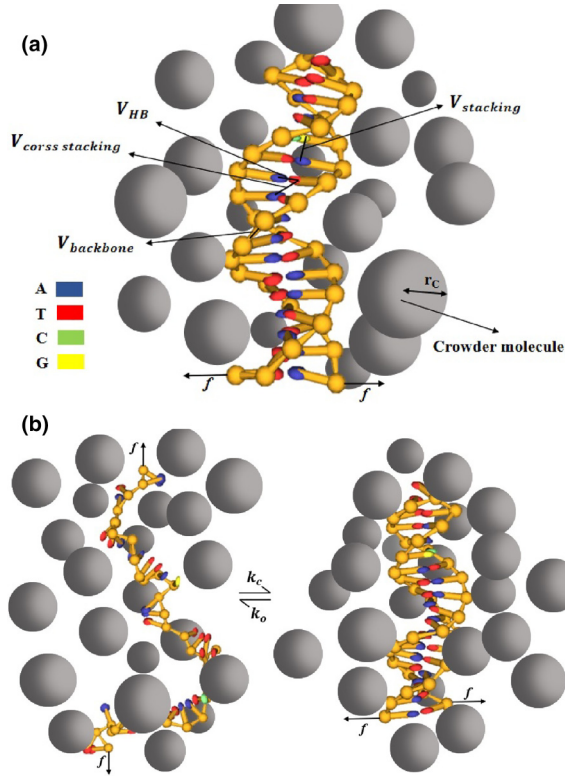


FIG. 2. Schematic illustration of the extended oxDNA model of a DNA hairpin in a crowded environment. (a) The DNA hairpin has a thymidine tetraloop and 15 bps in stem and its sequence is 5'-AAT ATT AAA TTA GAA TTTT TTC TAA TTT AAT ATT-3'. The radius of crowders  $r_c$  is 0.85nm. (b) The transition between the ssDNA and DNA hairpin in a crowded environment.

was used as a reference to measure the extension of the DNA construct. A piezo objective actuator was also used to adjust the focal plane during real-time measurements to cancel the mechanical drift of the microscope. Real-time image analysis was also carried out to get information on bead fluctuation and molecule extension by using the LabView software.

### B. Extended crowder-oxDNA model

OxDNA is a coarse-grained model that was originally developed by three scientists at the University of Oxford [26–28]. It has been widely used since reworked to treat the thermodynamics and mechanical properties of the DNA hairpin manipulated at a stretching force  $f$ . As illustrated in Fig. 2(a), this model treats a DNA strand as a chain of rigid bodies and captures the most relevant interactions of DNA, including the backbone connectivity ( $V_{\text{back}}$ ), hydrogen bonding between Watson-Crick complementary base pairs ( $V_{\text{H-bond}}$ ), stacking between adjacent bases pairs along the chain ( $V_{\text{stack}}$ ), cross stacking ( $V_{\text{cross-stack}}$ ), and the excluded volume interactions between base and backbone sites [29–31]. The complete forms for all potentials can be written as a sum of all the interaction terms as follows:

$$V = \sum_{\text{NN}} (V_{\text{back}} + V_{\text{stack}} + V'_{\text{exc}}) + \sum_{\text{other}} (V_{\text{H-bond}} + V_{\text{cross-stack}} + V_{\text{exc}}). \quad (1)$$

The electrostatic interactions were treated by using the Debye-Hückel approximation, with effective charges parameterized to reproduce the stability of short duplexes at sodium concentrations ranging from 0.1 to 1 M [32,33]. The interaction terms in Eq. (1), together with the electrostatic interactions, drive the formation of right-handed DNA helices and pairs in an antiparallel manner.

In the current paper, the extended ox-DNA model was further applied in crowding conditions [as indicated by Fig. 2(a)], where crowders with radius  $r_c$  were added to the simulation systems to mimic the macromolecules, such as PEG, in solution, while its volume fraction ( $\phi$ ) ranged from 0% to 20%. To account for the presence of the crowders, an interaction potential  $V_{\text{crowd,exc}}$  was introduced into the extended ox-DNA model, which includes the excluded volume interaction between two crowders ( $V_{\text{crowd-crowd}}$ ), between a crowder and a nucleotide's backbone site ( $V_{\text{crowd-back}}$ ), and between a crowder and the nucleotide's base site ( $V_{\text{crowd-base}}$ ), respectively. The general form of the excluded volume interaction potential can be expressed as follows:

$$f(r, \epsilon, \sigma, r^*) = \begin{cases} V_{LJ}(r, \epsilon, \sigma) & (r < r^*) \\ \epsilon V_{\text{smooth}}(r, b, r_{\text{cut}}) & (r^* < r < r_{\text{cut}}) \\ 0 & (\text{otherwise}). \end{cases} \quad (2)$$

This excluded volume interaction potential includes the Lennard-Jones potential  $V_{LJ}(r, \epsilon, \sigma) = 4\epsilon[(\frac{\sigma}{r})^{12} - (\frac{\sigma}{r})^6]$ , which was truncated by using the quadratic smoothing function  $V_{\text{smooth}}(r, b, r_{\text{cut}}) = b(r_{\text{cut}} - r)^2$  to guarantee that the excluded volume interaction potential is a differentiable function that is equal to 0 after a specified cutoff distance  $r_{\text{cut}}$ . The parameter  $r^*$  was equal to  $2r_c$  for the crowder-crowder interaction, and  $r_c + r_b$  for the interaction with the backbone site or the base site, where  $r_b$  corresponds to the radius of the backbone site or the base site in the oxDNA model, respectively. The crowder radius used in current simulations is  $r_c = 0.85\text{nm}$ , and the parameter values of  $\epsilon$ ,  $\sigma$ ,  $r^*$ ,  $b$ , and  $r_{\text{cut}}$  in the excluded volume potential are in terms of the simulation units of energy and distance, with one length unit equivalent to 8.518 Å, and one energy unit to 41.42pN nm. The scaled parameters in  $V_{\text{crowd-crowd}}$  were 2, 2.05, 2.0, 113.8, and 2.08, respectively, those in  $V_{\text{crowd-back}}$  were 2, 1.4, 1.35, 2897, and 1.42, respectively, and finally, those in  $V_{\text{crowd-base}}$  were 2, 1.22, 1.17, 17111, and 1.24, respectively.

The DNA hairpin [illustrated in Fig. 2(a)] used in the current simulations had 15 base pairs in the stem with double-helix structures and four bases in single-stranded loops. The mass, energy, and length units for the DNA hairpins used in the dynamics simulations were set as  $m_0 = 315.75Da$ ,  $\epsilon_0 = 4.142 \times 10^{-20}J$ , and  $l_0 = 8.518\text{Å}$ , respectively, which together determine the time unit as  $\tau_0 = (\epsilon_0/m_0 l_0^2)^{-\frac{1}{2}}$ . In the average-strength parametrizations that were used for all simulations, the strengths of interactions  $V_{\text{stack}}$  and  $V_{\text{H-bond}}$  were set to be the same for all types of nucleotides, and were also parameterized to reproduce melting thermodynamics of hairpins with average-sequence content as predicted by SantaLucia's nearest-neighbor model [33]. The evolution of the system was realized by solving the Newton's equation of motion using the velocity Verlet algorithm. Then the velocities and angular velocities of each particle were updated

from a Maxwell-Boltzmann distribution at each temperature. Brute-force closing simulations, as well as the forward-flux sampling, were performed to study the kinetics of the hairpin formation. The forward-flux sampling, a rare event method, was used to accelerate the kinetic measurements [29,30]. The conformation transition between the folded and unfolded states is demonstrated in Fig. 1(b), which was carried out at different stretching forces at the temperature value of 310 K.

### III. RESULTS AND DISCUSSIONS

#### A. Dynamics of DNA hairpin under macromolecule crowding conditions

As can be observed in Fig. 1, the hairpin construct undergoes a series of transitions with the increasing stretching force from almost zero to 70.0 pN by moving the permanent magnet pair closer to the sample. At a force of about 11.7 pN, the extension suddenly increased with a stepsize of  $\sim 14$  nm, indicating the unfolding of DNA hairpin to single stranded DNA (ssDNA). After that, the extension of DNA gradually increased until the overstretching transition occurred at  $\sim 65$  pN, which showed a sudden extension increase of  $\sim 130$  nm, that is consistent with the overstretching transition of the dsDNA handles.

When the stretching force was reduced to below 11.7 pN, the folding-unfolding transition was reversible at the applied experimental conditions, so the dynamics process of the unfolding-folding transition of DNA hairpin at different stretching forces can be recorded [Figs. 3(a)–3(c)]. At every constant stretching force, the extension-time curve has two distinct states of DNA hairpin indicated by long and short extensions, representing the unfolded ssDNA state and the folded hairpin state. The extension probability distribution in the right panels has two clear peaks separated by a distance of  $\sim 13$  nm, which corresponds to the displacement difference of the folded hairpin state and unfolded ssDNA state along the direction of the stretching force. With the increasing stretching force from 10.33 pN to 11.34 pN, the time of the DNA hairpin staying at a folded state was prominently reduced, which demonstrated that the increasing stretching force tended to destabilize the DNA hairpin.

To investigate the impact of the detected macromolecule crowding on the stability of the DNA hairpin, the PEG 8000 macromolecule was added to the experimental buffer and its wt% concentration ranged from 2.5% to 10%. As displayed in Figs. 3(c)–3(e), at the constant stretching force of 11.34 pN, the increasing concentration of macromolecule PEG 8000 induced DNA hairpin stay at folded state with higher probability. As a result, it can be inferred that macromolecule crowding caused by macromolecule PEG 8000 enhanced the stability of the DNA hairpin. When the macromolecule PEG 8000 in the experiment buffer was replaced by macromolecule PEG 400, similar results were also observed.

According to the extension probability distribution, the free-energy landscape of the DNA hairpin can be obtained. More specifically, the free energy  $F$  was subjected to the modulation of stretching force  $f$ , and can be expressed as follows:  $F = H - TS - fX$ , where  $T$ ,  $H$ , and  $S$  refer to the absolute temperature, enthalpy, and entropy, respectively. The

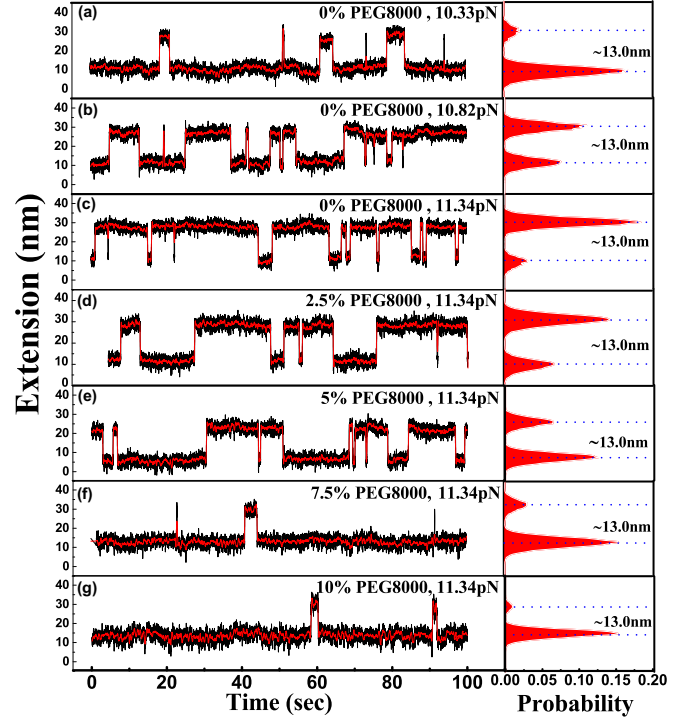


FIG. 3. Dynamics of the DNA hairpin at different stretching forces and crowding conditions. [(a)–(c)] Extension time courses of the DNA hairpin were measured in a solution of 150 mM NaCl, 10 mM Tris, pH 7.2, at forces of 10.33 pN, 10.82 pN, and 11.34 pN, respectively. (C ~ G) Extension time courses of DNA hairpin at 11.34 pN were measured in the same solution with the concentration of PEG 8000 ranging from 0% to 10%. The right panels show the corresponding extension probability distribution with two distinct peaks separated by  $\sim 13$  nm.

free energy  $F_c = H_c - TS_c - fX_c$  and  $F_o = H_o - TS_o - fX_o$  separately correspond to those in the folded hairpin state and unfolded ssDNA states, where  $X_c$  and  $X_o$  stand for the displacement of the folded hairpin and unfolded ssDNA states along the direction of extension. Thus, the free energy difference between two states can be expressed as follows:  $\Delta F = F_o - F_c = \Delta H - T\Delta S - f\Delta X$  and the open probability at the unfolded ssDNA state  $P_o(f)$  was defined as the percentage of time at unfolded ssDNA state [34], which is force dependent and can be expressed as follows:

$$P_o(f) = \frac{e^{-\frac{F_o}{k_B T}}}{e^{-\frac{F_o}{k_B T}} + e^{-\frac{F_c}{k_B T}}} = \frac{1}{1 + e^{\frac{\Delta F}{k_B T}}} \quad (3)$$

The free-energy landscape at the critical force should be symmetric, namely,  $\Delta F(f = f_{\text{crit}}) = \Delta H - T\Delta S - f_{\text{crit}}\Delta X = 0$ . Hence,  $\Delta H - T\Delta S = f_{\text{crit}}\Delta X$  was obtained. Consequently, the free energy difference can be rewritten as follows:  $\Delta F(f) = (f_{\text{crit}} - f)\Delta X$ , where  $\Delta X = x_c + x_o$  is constant around room temperature. Thus, the open probability  $P_o(f)$  can be reexpressed as follows:

$$P_o(f) = \frac{1}{1 + e^{(f_{\text{crit}} - f)\Delta X/k_B T}}. \quad (4)$$

This two-state Boltzmann relationship was used to fit the open probability obtained from the single-molecule experiment

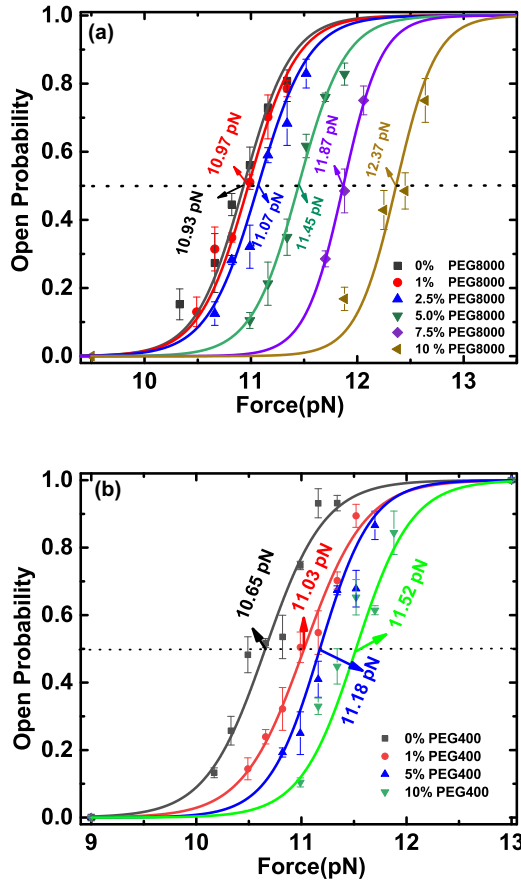


FIG. 4. Force-dependent open probability of DNA hairpin in experiment buffer with different concentrations of PEG 8000 (a) and PEG 400 (b). Fitting with the two-state Boltzmann relationship gives the critical forces at  $P_o(f) = 50\%$ .

under different macromolecule crowding conditions. As shown in Figs. 4(a) and 4(b) the critical forces under different crowding conditions can be obtained at  $P_o(f) = 50\%$ . For example, the critical force of the DNA hairpin in 10% PEG 8000 was 12.37pN, and the critical forces increase by increasing the concentration of PEG 8000. The critical forces changing with the increasing concentration of PEG 400 macromolecules also follow similar rules.

The folded (unfolded) states correspond to two local minimal free-energy states in the free-energy landscape of the DNA hairpin and transfer to each other by crossing the transition state with the force-dependent unfolding rate  $k_o(f) = k_o^0 \exp(fx_o/k_B T)$  and folding rate  $k_c(f) = k_c^0 \exp(-fx_c/k_B T)$  [35,36], where  $x_c$ ,  $x_o$ ,  $k_B$ , and  $T$  represent the distances to the transition point from the folded and unfolded states, the Boltzmann constant, and the absolute temperature, respectively. The logarithm of the folding-unfolding rates can be expressed as follows:

$$\begin{aligned} \ln k_o(f) &= \ln k_o^0 + (x_o/k_B T)f, \\ \ln k_c(f) &= \ln k_c^0 - (x_c/k_B T)f, \end{aligned} \tag{5}$$

which were used to fit linear functions of force in the force range close to the equilibrium critical force and their cross point of the unfolding (folding) rates gives the equilibrium

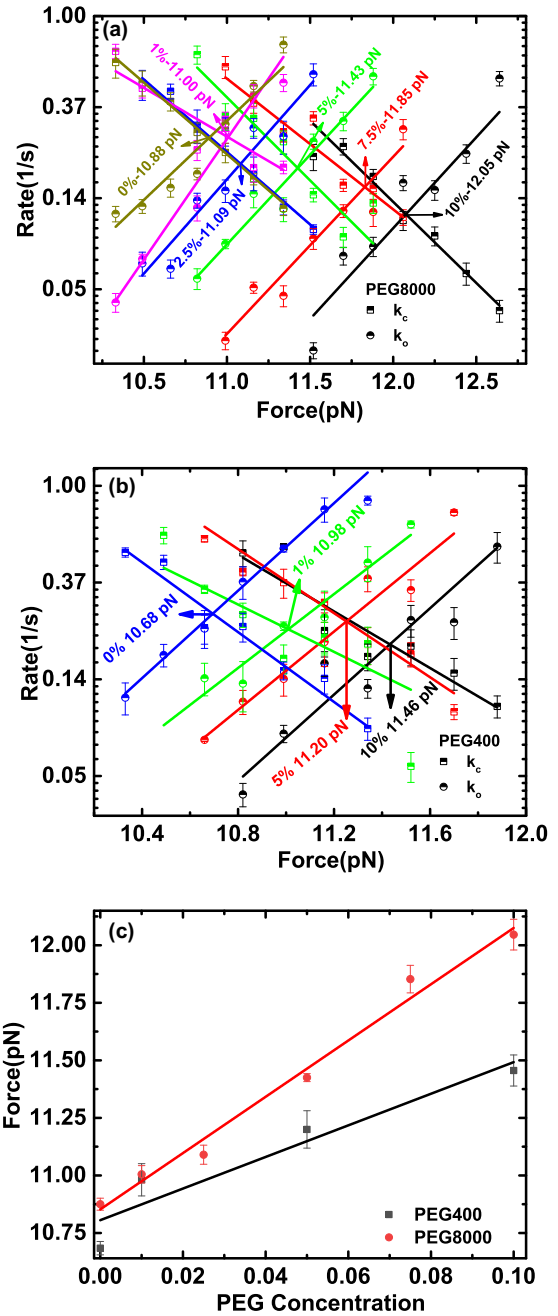


FIG. 5. Force-dependent folding and unfolding rates of DNA hairpin in the experimental solution with different concentrations of PEG 8000 (a) and PEG 400 (b). The cross points indicated by different color arrows give the critical forces, which are consistent with the analysis of the force-dependent open probability of the DNA hairpin. (c) The critical forces as a function of the PEG concentration and its dependence on the molecular weight of PEG.

critical force. As can be ascertained from Figs. 5(a) and 5(b), the cross points of the unfolding (folding) rates indicated by color arrows separately give the critical forces of the DNA hairpin in experiment buffer with different concentration values of the PEG 8000 and PEG 400 macromolecules. It is interesting to note that all of them are consistent with the analysis of force-dependent open probability shown in Figs. 4(a) and 4(b). Finally, the generalized dependence of the critical

forces on the concentration of the PEG 8000 and PEG 400 macromolecules is outlined in Fig. 5(c). Obviously, the critical forces linearly pertain to the increasing concentration of the PEG 8000 or PEG 400 macromolecules. As the same time, the critical forces of the DNA hairpin at the same wt% concentration of PEG macromolecule are strongly dependent on the molecular weight of PEG, namely, the critical forces of the DNA hairpin in the solution with the PEG 8000 are relatively larger than those in the solution with the PEG 400.

For a DNA hairpin staying at the folded state, the unfolding probability as a function of time is defined as the probability for the unfolding transition to occur at least once within the time period. The folding probability can be defined similarly. During the conformation fluctuation at constant forces, the dwell time at each state determines the transition rates. The folding-unfolding probabilities as a function of time were obtained by analyzing the cumulative distribution of the dwell time, which can be fitted by an exponential function of  $p(t) = 1 - \exp(-kt)$  [34], which can yield the transition rates of  $k_o$  and  $k_c$ .

As shown in Figs. 6(a) and 6(b) at a constant stretching force of 11.34 pN, the folding-unfolding probabilities of the DNA hairpin as a function of time is strongly subjected to the concentration of the PEG 8000 macromolecule ranging from 0% to 10%, which was further proven by a significant enhancement in the folding rate and a concomitant reduction in the unfolding rate upon increasing the amounts of the PEG 8000 macromolecule [(depicted in the insets of Figs. 6(a) and 6(b)]. The folding rate  $k_c$  increased from  $0.121 \text{ s}^{-1}$  in the solution without PEG 8000 to  $0.433 \text{ s}^{-1}$  in only 10% PEG 8000. In contrast, the unfolding rate  $k_o$  decreased from  $0.731 \text{ s}^{-1}$  in the solution without PEG 8000 to  $0.022 \text{ s}^{-1}$  in 10% PEG 8000. These changes in the folding-unfolding rates resulted in the equilibrium constant  $k_{\text{eq}} = \frac{k_c}{k_o}$  shifts by more than two orders of magnitude in favor of the folded hairpin state in only 10% PEG 8000.

Figures 6(c) and 6(d) demonstrate the folding-unfolding probabilities of the DNA hairpin as a function of time at different concentration values of PEG 400 macromolecules, and their respective insets provide the folding-unfolding rates as a function of the concentration of PEG 400. At the same constant stretching force 11.34 pN, the dependence of the unfolding rate  $k_o$  on the concentration of PEG 400 was similar to that of PEG 8000, namely, the unfolding rate  $k_o$  was reduced from  $0.859 \text{ s}^{-1}$  in the buffer without PEG 400 to  $0.123 \text{ s}^{-1}$  in only 10% PEG 400. Nonetheless, the folding rate  $k_c$  as a function of the concentration of the PEG 400 macromolecule was totally different from that of the PEG 8000 macromolecule shown in the inset of Fig. 6(a). The folding rate  $k_c$  was enhanced up to  $0.195 \text{ s}^{-1}$  in a buffer with 1% PEG 400 from  $0.081 \text{ s}^{-1}$  in a buffer without PEG 400. However, it was not further increased by increasing amounts of PEG 400 macromolecule to the experimental buffer. Consequently, the equilibrium constant  $k_{\text{eq}} = \frac{k_c}{k_o}$  shifts by one order of magnitude in favor of the folded hairpin state in only 10% PEG 400 mainly originated from the reduction of the unfolding rate  $k_o$ .

The implementation of the magnetic tweezers-based results in the development of the critical forces of the DNA

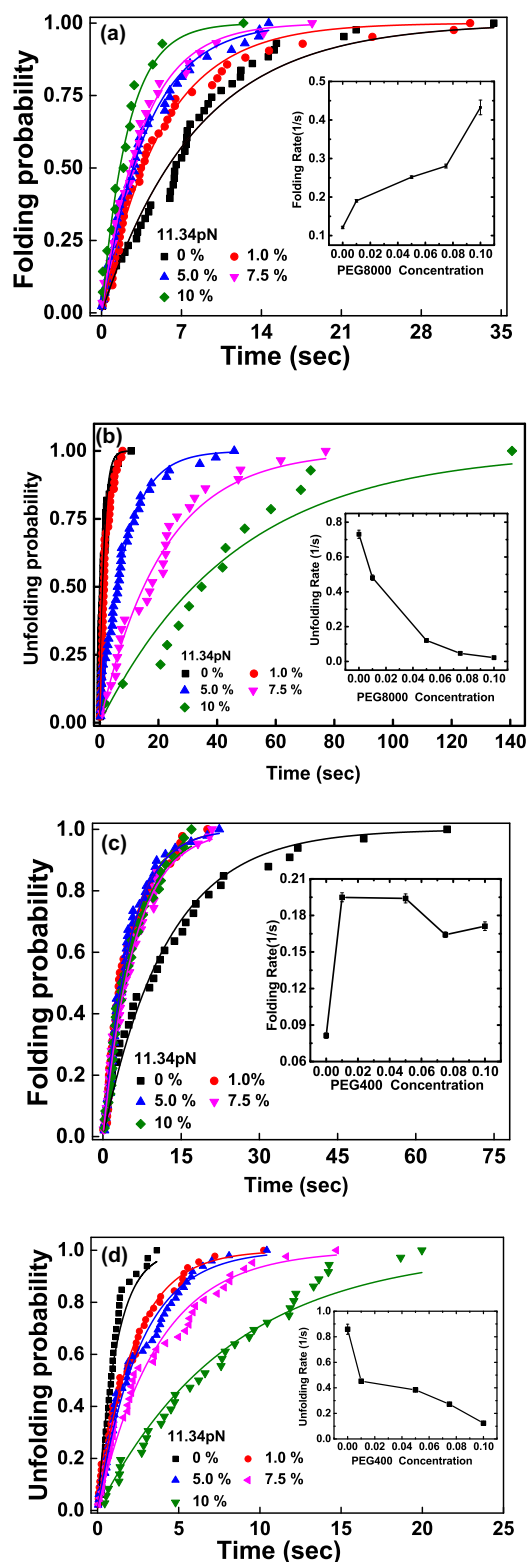


FIG. 6. Distribution of the folding-unfolding probabilities are shown as a function of time in a solution with different PEG concentration values at a stretching force of 11.34 pN. Fitting with exponential function  $p(t) = 1 - \exp(-kt)$  gives the folding-unfolding rates at different PEG concentration values and their dependence on the concentration of the PEG 8000 and PEG 400 macromolecules are shown in their insets.

hairpins in different crowding conditions that linearly pertain to the increasing PEG concentrations. In addition, they are totally different from the nonlinear behaviors on the increasing dextran concentration using atomic force microscopy-based single cell force spectroscopy [37]. Generally, the macromolecule crowding effects are expected to promote macromolecular complexation by the excluded volume effects. However, by comparing the proposed magnetic tweezers-based experiment and the recent single-cell experiments in the literature, a discrepancy between the macromolecule crowding effects caused by different macromolecules was found, which will be further clarified based on the extended crowder-oxDNA model.

### B. Simulation results

In the extended crowder-oxDNA model, crowders were added to simulated systems to mimic the macromolecule crowding, the impact of crowders on the kinetic behavior of the DNA hairpin will be further explored to clarify the above-mentioned discrepancies. DNA hairpin with a thymidine tetraloop and 15 bps in its stem was used to perform simulations. Its kinetic behaviors in different crowding conditions, with volume fractions ranging from 0 to 20% and the crowder radius  $r_c$  of 0.85 nm, were successfully reproduced and the extension-time curves of the DNA hairpin in the simulation systems with a volume fraction of 0% and 5% were demonstrated in Fig. 7, in which the extension-time curve at a constant stretching force transitioned between the unfolded ssDNA and the folded hairpin states. Moreover, the extension probability distribution in their right panel exhibited two clear peaks separated by a distance of about 12.5 nm. By taking into account the stretching force, this distance was reasonably consistent with the contour length of the single-stranded nucleotide.

The dynamics of the DNA hairpin depends on the stretching forces and the volume fractions of crowders in the simulated systems. Figs. 7(a)–7(e) demonstrate the dynamics of the DNA hairpin in the simulated systems without crowders. As a comparison, Figs. 7(f)–7(j) indicate those in the simulated systems with volume fraction  $\phi = 5\%$ . Obviously, their common features are that the increasing stretching forces make the DNA hairpin prone to stay at an unfolded ssDNA state. However, the stretching force, at which the DNA hairpin has roughly equal probability to stay at the folded hairpin and the unfolded ssDNA states, was increased from about 6.81 pN to 7.05 pN, indicating that the addition of crowders to the simulated systems enhanced the stability of the DNA hairpin.

The force-dependent open probability and the folding-unfolding rates changing with the stretching force can be identified from the dynamics of the DNA hairpin in different crowding conditions, such as those at volume fractions of 0% and 5% in Fig. 7. Figure 8(a) depicts the fitting curves of the force-dependent open probability by Eq. (2) and the critical forces at  $P_o(f) = 50\%$ , which were gradually enhanced from 6.67 pN to 8.30 pN with the increasing volume fractions from 0% to 20%. The dependence of the folding-unfolding rates in different crowding conditions on the stretching forces and their fitting lines by Eq. (3) are demonstrated in Fig. 8(b). At the cross points indicated by different color arrows, the

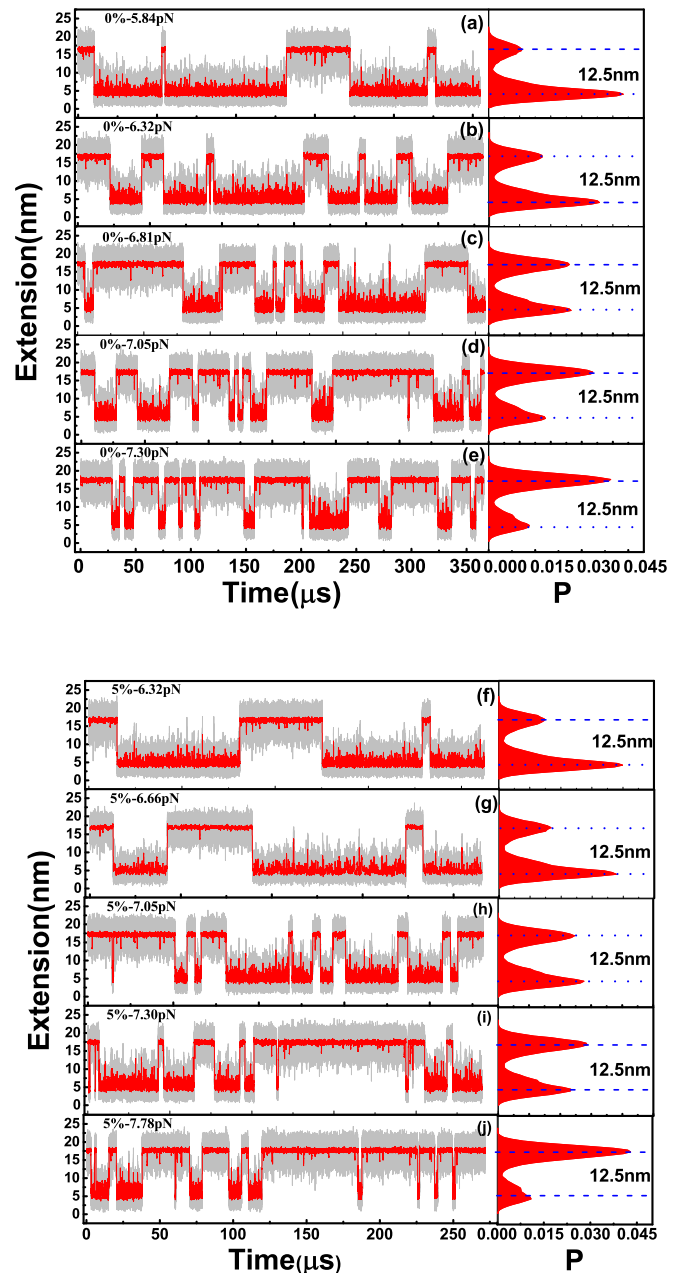


FIG. 7. Dynamics of the DNA hairpin at different stretching forces and crowding conditions. Extension time courses of the DNA hairpin were measured in simulated systems with volume fractions of 0% [(a)–(e)] and 5% [(f)–(j)]. The right panels show their corresponding extension probability distribution with two distinct peaks separated by  $\sim 12.5$  nm.

folding rate was equal to the unfolding rate and the corresponding stretching forces are the critical forces at the different volume fractions from 0% to 20%; all of these are totally consistent with the analysis based on the force-dependent open probability and, more importantly, the linear dependence of the critical forces on the increasing volume fractions, as shown in the inset of Fig. 8(b), is reasonably consistent with the single-molecule experimental results in Fig. 5(c).

As pointed out by a recently reported single-molecule experiment [38], the stability of the DNA hairpin depends on its

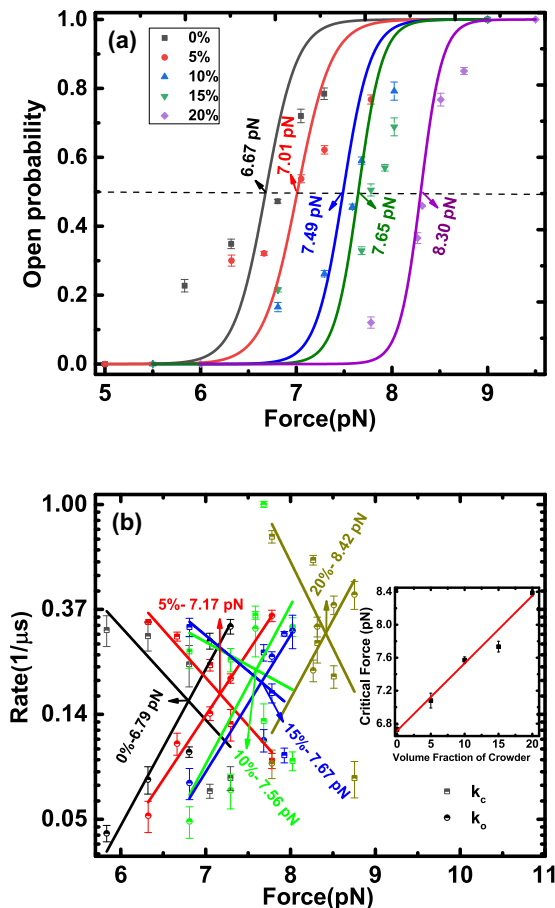


FIG. 8. In simulation systems with increasing volume fractions from 0% to 20%. (a) Force-dependent open probability of the DNA hairpin versus stretching force, fitting with the two-state Boltzmann relationship gives the critical forces. (b) The dependence of the force-dependent folding-unfolding rates of the DNA hairpin on the stretching forces. The cross points indicated by different color arrows give the critical forces, which are consistent with the analysis of the force-dependent open probability of the DNA hairpin.

stem length, loop length, and the GC content in the stem of the DNA hairpin. To enhance the simulation speed, the sequence of the DNA hairpin used in the magnetic tweezers-based experiment was replaced by sequence 5'-AAT ATT AAA TTA GAA TTTT TTC TAA TTT AAT ATT-3' to perform simulations, in which the GC content in the stem of the DNA hairpin was reduced to 6.7% from 60%, and the loop size was also reduced to 4 nt from 8 nt. Its corresponding critical force at a volume fraction of 0%, as shown Fig. 8(b), was about 6.67pN, which was reasonably consistent with the previous obtained single-molecule experiment value of DNA hairpin with a similar sequence [38]. This sequence replacement does not alter the linear dependence of the critical forces of the DNA hairpin on the increasing volume fractions.

#### IV. CONCLUSIONS AND PERSPECTIVES

In this paper, a magnetic tweezers-based experiment in combination with simulations based on the crowder-oxDNA model was applied to identify the discrepancies among the

macromolecule crowding effects caused by different macromolecules, such as PEG and dextran. The incorporation of the PEG 8000 or PEG 400 macromolecules into the experiment buffer enhanced the stability of the DNA hairpin. The critical forces of the DNA hairpin in the experimental buffer with different concentration values of the PEG 8000 or PEG 400 macromolecules were separately identified by force-dependent open probability and the folding-unfolding rates, which were reasonably consistent with each other and linearly pertained to the increasing PEG concentrations. Nevertheless, the critical force of the DNA hairpin in the experimental buffer with the PEG 8000 macromolecule was obviously larger than that in experimental buffer with the PEG 400 macromolecule at the same concentration.

The magnetic tweezers exhibited high precision and stability, by which the dependence of the folding rates changing with the PEG concentration on the molecule weight could be accurately identified. From the previously reported FRET-based experiments in the literature, it was pointed out that the folding rates increased with increasing PEG concentration and decreased for the unfolding rates, which was universal for the PEG 8000 and PEG 400 macromolecules. By means of contrast, from the proposed current magnetic tweezers-based experiments, it was found that the folding rates changing with the concentration of PEG was dependent on the molecule weight. At a constant stretching force of 11.34 pN, by increasing PEG concentration from 0% to 10%, the folding rate of the DNA hairpin in the experimental buffer with the PEG 8000 was gradually increased. However, in the experimental buffer with the 1% PEG 400 macromolecule, it was first enhanced up to  $0.195 s^{-1}$  from  $0.081 s^{-1}$  in the experiment buffer without PEG 400, but it did not further increase by increasing the amounts of PEG 400 to the experimental buffer. As far as the unfolding rate of the DNA hairpin  $k_o$  in the experimental buffer with either the PEG 8000 or PEG 400 macromolecules is concerned, both of which were gradually reduced, an independency on the molecule weight of PEG was detected.

The magnetic tweezer-based experiment results were further compared with the simulated outcomes based on the extended crowder-oxDNA model. In the extended crowder-oxDNA model, the crowdors were added to the simulated systems to mimic the behavior of macromolecules, as well as the interactions between the two crowdors, between the crowder and the nucleotides backbone site, and between the crowder and the nucleotides base site, which were described by the excluded volume interactions. By increasing the volume fractions from 0% to 20%, the stability of the DNA hairpin was obviously enhanced and the critical forces were linearly associated with the increasing volume fractions of crowdors, which is in direct agreement with the magnetic tweezer-based experimental results. Thereby, it can be argued that the excluded volume interactions (also known as the depletion effects) are mainly responsible for the interaction between the PEG macromolecule and the DNA hairpin. In striking contrast, the nonlinear behaviors in atomic force microscopy-based single cell force spectroscopy cannot be solely explained by the excluded volume interactions, and other nonspecific interactions, such as the associative interactions, should be also taken into account.

The combination of the magnetic tweezers-based experiment and simulations based on the crowder-oxDNA model opens a path to further investigate the macromolecule crowding effects. The interaction potential between the crowder and the DNA hairpin can be tuned according to the physical characters of the inert, synthetic molecule, such as dextran and Ficoll, and then the crowder-oxDNA model could provide the open probability, folding-unfolding rates, and critical forces of DNA hairpins in different crowded environments. These outcomes will be further compared with the results obtained in single-molecule experiments based on magnetic tweezers. As a result, the interaction between an inert, synthetic molecule, and the DNA hairpin could be substantially understood, which is of great importance to mimic the cytosolic environments using mixtures of the different inert molecules.

#### ACKNOWLEDGMENTS

This research was supported by the National Natural Science Foundation of China under Grants No. 11864006, No. 12174322, No. 12164007, and No. 12204118, Guizhou Scientific and Technological Program [No. 20185781, No. ZK(2021)004, No. ZK(2021)032 and No. 20185781-15], the Foundation of Key Laboratory of Animal Genetics, Breeding and Reproduction in The Plateau Mountainous Region, Ministry of Education, Guizhou University (No. KY2020243), Guizhou Provincial Graduate Scientific Research Foundation (No. YJSKYJJ(2021)066). We are also thankful for the computing support of the State Key Laboratory of Public Big Data, Guizhou University.

- 
- [1] M. A. Mourão, J. B. Hakim, S. Schnell, Connecting the dots: The effects of macromolecular crowding on cell physiology, *Biophys. J.* **107**, 2761 (2014).
- [2] A. H. Elcock, Models of macromolecular crowding effects and the need for quantitative comparisons with experiment, *Curr. Opin. Struct. Biol.* **20**, 196 (2010).
- [3] S. Nakano, D. Miyoshi, and N. Sugimoto, Effects of molecular crowding on the structures, interactions, and functions of nucleic acids, *Chem. Rev.* **114**, 2733 (2014).
- [4] J. van den Berg, A. J. Boersma, and B. Poolman, Microorganisms maintain crowding homeostasis, *Nat. Rev. Microbiol.* **15**, 309 (2017).
- [5] C. Li, X. Zhang, M. Dong, and X. Han, Progress on crowding effect in cell-like structures, *Membranes* **12**, 593 (2022).
- [6] S. Matsumoto and N. Sugimoto, New insights into the functions of nucleic acids controlled by cellular microenvironments, *Top. Curr. Chem. (Z)* **379**, 17 (2021).
- [7] H. X. Zhou, G. Rivas, and A. P. Minton, Macromolecular crowding and confinement: Biochemical, biophysical, and potential physiological consequences, *Annu. Rev. Biophys.* **37**, 375 (2008).
- [8] X. Ge, D. Luo, and J. Xu, Cell-free protein expression under macromolecular crowding conditions, *PLoS ONE* **6**, e28707 (2011).
- [9] M. S. Aporvari, S. Dang, J. Marfai, K. Coursey, R. McGorty, R. M. Robertson-Anderson, Crowding and confinement act in concert to slow DNA diffusion within cell-sized droplets, *iScience* **25**, 105122 (2022).
- [10] D. Miyoshi and N. Sugimoto, Molecular crowding effects on structure and stability of DNA, *Biochimie* **90**, 1040 (2008).
- [11] N. Biswas, M. Ichikawa, A. Datta, Y. T. Sato, M. Yanagisawa, and K. Yoshikawa, Phase separation in crowded microspheroids: DNA-PEG system, *Chem. Phys. Lett.* **539-540**, 157 (2012).
- [12] J. Groen, D. Foschepoth, E. te Brinke, A. J. Boersma, H. Imamura, G. Rivas, H. A. Heus, and W. T. Huck, Associative interactions in crowded solutions of biopolymers counteract depletion effects, *J. Am. Chem. Soc.* **137**, 13041 (2015).
- [13] S. Hou, P. Trochimczyk, L. Sun, A. Wisniewska, T. Kalwarczyk, X. Zhang, B. Wielgus-Kutrowska, A. Bzowska, and R. Holyst, How can macromolecular crowding inhibit biological reactions? The enhanced formation of DNA nanoparticles, *Sci. Rep.* **6**, 22033 (2016).
- [14] J. Shin, A. G. Cherstvy, and R. Metzler, Polymer looping is controlled by macromolecular crowding, spatial confinement, and chain stiffness, *ACS Macro Lett.* **4**, 202 (2015).
- [15] G. D'Adamo and C. Micheletti, Molecular crowding increases knots abundance in linear polymers, *Macromolecules* **48**, 6337 (2015).
- [16] M. Zoli, DNA size in confined environments, *Phys. Chem. Chem. Phys.* **21**, 12566 (2019).
- [17] O. Stiehl, K. Weidner-Hertrampf, and M. Weiss, Kinetics of conformational fluctuations in DNA hairpin-loops in crowded fluids, *New J. Phys.* **15**, 113010 (2013).
- [18] L. E. Baltierra-Jasso, M. J. Morten, L. Laflor, S. D. Quinn, and S. W. Magennis, Crowding-induced hybridization of single DNA hairpins, *J. Am. Chem. Soc.* **137**, 16020 (2015).
- [19] H. L. Sung and D. J. Nesbitt, Effects of molecular crowders on single-molecule nucleic acid folding: Temperature-dependent studies reveal true crowding vs enthalpic interactions, *J. Phys. Chem. B* **125**, 13147 (2021).
- [20] N. F. Dupuis, E. D. Holmstrom, and D. J. Nesbitt, Molecular-crowding effects on single-molecule RNA folding (unfolding) thermodynamics and kinetics, *Proc. Natl. Acad. Sci. USA* **111**, 8464 (2014).
- [21] J.-M. Yuan, C.-L. Chyan, H.-X. Zhou, T.-Y. Chung, H. Peng, G. Ping, and G. Yang, The effects of macromolecular crowding on the mechanical stability of protein molecules, *Protein Sci.* **17**, 2156 (2008).
- [22] X. Zhang, H. Chen, H. Fu, P. S. Doyle, and J. Yan, Two distinct overstretched DNA structures revealed by single-molecule thermodynamics measurements, *Proc. Natl. Acad. Sci. USA* **109**, 8103 (2012).
- [23] X. Zhang, H. Chen, S. Le, I. Rouzina, P. S. Doyle, and J. Yan, Revealing the competition between peeled ssDNA, melting bubbles, and S-DNA during DNA overstretching by single-molecule calorimetry, *Proc. Natl. Acad. Sci. USA* **110**, 3865 (2013).
- [24] Y. Xu, H. Chen, Y. J. Qu, A. Kefremov, M. Li, Z. C. Ouyang, D. S. Liu, and J. Yan, Mechano-chemical selections of two

- competitive unfolding pathways of a single DNA i-motif, *Chin. Phys. B* **23**, 068702 (2014).
- [25] Z. J. Yang, G. H. Yuan, W. L. Zhai, J. Yan, and H. Chen, The kinetics of force-dependent hybridization and strand-peeling of short DNA fragments, *Sci. China Phys. Mech. Astron.* **59**, 680013 (2016).
- [26] T. E. Ouldridge, A. A. Louis, and J. P. Doye, Structural, mechanical, and thermodynamic properties of a coarse-grained DNA model, *J. Chem. Phys.* **134**, 085101 (2011).
- [27] F. Hong, J. S. Schreck, and P. Šulc, Understanding DNA interactions in crowded environments with a coarse-grained model, *Nucleic Acids Res.* **48**, 10726 (2020).
- [28] J. S. Schreck, T. E. Ouldridge, F. Romano, P. Šulc, L. P. Shaw, A. A. Louis, and J. P. Doye, DNA hairpins destabilize duplexes primarily by promoting melting rather than by inhibiting hybridization, *Nucleic Acids Res.* **43**, 6181 (2015).
- [29] P. Šulc, F. Romano, T. E. Ouldridge, L. Rovigatti, J. P. Doye, and A. A. Louis, Sequence-dependent thermodynamics of a coarse-grained DNA model, *J. Chem. Phys.* **137**, 135101 (2012).
- [30] B. E. Snodin, F. Randisi, M. Mosayebi, P. Šulc, J. S. Schreck, F. Romano, T. E. Ouldridge, R. Tsukanov, E. Nir, A. A. Louis, J. P. Doye, Introducing improved structural properties and salt dependence into a coarse-grained model of DNA, *J. Chem. Phys.* **142**, 234901 (2015).
- [31] L. Li, H. Wang, C. Xiong, D. Luo, H. Chen, and Y. Liu, Quantify the combined effects of temperature and force on the stability of DNA hairpin, *J. Phys.: Condens. Matter* **33**, 185102 (2021).
- [32] J. Mazur and R. L. Jernigan, Distance-dependent dielectric constants and their application to double-helical DNA, *Biopolymers* **31**, 1615 (1991).
- [33] J. SantaLucia and D. Hicks, The thermodynamics of DNA structural motifs, *Annu. Rev. Biophys. Biomol. Struct.* **33**, 415 (2004).
- [34] C. Liu, W. Zhai, H. Gong, Y. Liu, and H. Chen, Effect of fluoride ion on the stability of DNA hairpin, *Chem. Phys. Lett.* **678**, 35 (2017).
- [35] G. I. Bell, Models for the specific adhesion of cells to cells, *Science* **200**, 618 (1978).
- [36] M. Rico-Pasto, I. Pastor, and F. Ritort, Force feedback effects on single molecule hopping and pulling experiments, *J. Chem. Phys.* **148**, 123327 (2018).
- [37] P. Steffen, C. Verdier, and C. Wagner, Quantification of Depletion-Induced Adhesion of Red Blood Cells, *Phys. Rev. Lett.* **110**, 018102 (2013).
- [38] M. T. Woodside, W. M. Behnke-Parks, K. Larizadeh, K. Travers, D. Herschlag, and S. M. Block, Nanomechanical measurements of the sequence-dependent folding landscapes of single nucleic acid hairpins, *Proc. Natl. Acad. Sci. USA* **103**, 6190 (2006).